NeuroImage: Clinical 28 (2020) 102447

Contents lists available at ScienceDirect

NeuroImage: Clinical

journal homepage: www.elsevier.com/locate/ynicl

Quantitative MRI demonstrates abnormalities of the third ventricle subventricular zone in neurofibromatosis type-1 and sporadic paediatric optic pathway glioma

Natalie R. Boonzaier [a,1], Patrick W. Hales [a,*,1], Felice D'Arco [b], Bronwen C. Walters [b], Ramneek Kaur [a], Kshitij Mankad [b], Jessica Cooper [b], Alki Liasis [b,c], Victoria Smith [b], Patricia O'Hare [b], Darren Hargrave [a,b], Christopher A. Clark [a]

[a] Developmental Imaging and Biophysics Section, Developmental Neurosciences, University College London Great Ormond Street Institute of Child Health, London, UK
[b] Great Ormond Street Hospital for Children NHS Foundation Trust, London, UK
[c] University of Pittsburgh Medical Center, Children's Hospital of Pittsburgh, Pittsburgh, USA

ARTICLE INFO

Keywords:
Optic pathway glioma
Third ventricle subventricular zone
Neurofibromatosis type-1
Quantitative magnetic resonance imaging
Paediatric

ABSTRACT

Background: The subventricular zone of the third ventricle (TVZ) is a germinal stem cell niche, identified as the possible location of optic pathway glioma (OPG) cell origin. Paediatric OPGs are predominantly diagnosed as low-grade astrocytomas, which are either sporadic or are associated with neurofibromatosis type-1 (NF1). These tumours often cause a significant impairment to visual acuity (VA). Infiltrative/invasive tumour activity is associated with increased apparent diffusion coefficient (ADC) and cerebral blood flow (CBF). This study aimed to determine whether TVZ imaging features differed between sporadic-OPG, NF1-OPG and controls, and whether the ADC and CBF profile at the germinal stem cell niche (the TVZ) correlated with the primary outcome of VA.
Methods: ADC and CBF MRI data were acquired from 30 paediatric OPG patients (median age 6 years; range 8 months–17 years), along with VA measurements, during clinical surveillance of their tumour. Values for mean ADC and maximum CBF were measured at the TVZ, and normalized to normal-appearing grey matter. These values were compared between the two OPG groups and the healthy control subjects, and multivariate linear regression was used to test the linear association between these values and patient's VA.
Results: In the TVZ, normalized mean ADC was higher in NF1-associated OPG patients ($N = 15$), compared to both sporadic OPG patients ($N = 15$; $p = 0.010$) and healthy controls ($N = 14$; $p < 0.001$). In the same region, normalized maximum CBF was higher in sporadic OPG patients compared to both NF1-OPG patients ($p = 0.016$) and healthy controls ($p < 0.001$). In sporadic OPG patients only, normalized mean ADC in the TVZ was significantly correlated with visual acuity ($R^2 = 0.41$, $p = 0.019$). No significant correlations were found between TVZ CBF and ADC values and visual acuity in the NF1-associated OPG patients.
Conclusion: Quantitative MRI detects TVZ abnormalities in both sporadic and NF1-OPG patients, and identifies TVZ features that differentiate the two. TVZ features may be useful MRI markers of interest in future predictive studies involving sporadic OPG.

1. Introduction

Optic pathway gliomas (OPG) in children are predominantly diagnosed as WHO grade I pilocytic astrocytomas (PA), and are often associated with neurofibromatosis type 1 (NF1), an autosomal dominant condition that predisposes patients to tumour formation (Lee et al., 2010a). The remaining OPGs are classed as sporadic. Generally, NF1-associated OPGs are clinically less aggressive over time, while sporadic OPGs are more likely to progress, both radiologically (tumour growth) and clinically (visual function decline). Paediatric OPG survival rates are high, and surveillance includes regular MRI to assess tumour growth and ophthalmologic assessment to evaluate visual function

* Corresponding author at: Developmental Imaging & Biophysics Section, UCL Great Ormond Street Institute of Child Health, 30 Guilford Street, London WC1N 1EH, UK.
E-mail address: p.hales@ucl.ac.uk (P.W. Hales).
[1] Equally contributing first authors.

https://doi.org/10.1016/j.nicl.2020.102447
Received 20 May 2019; Received in revised form 17 September 2020; Accepted 20 September 2020
Available online 28 September 2020

(Listernick et al., 2007). Sporadic OPGs are more often located at the optic chiasm and tracts, as opposed to the NF1-associated preferred location of the optic nerves (Kornreich et al., 2001). NF1-associated and sporadic PAs are histologically similar. However, their tumourigenesis and underlying molecular mechanisms of pathology are different. NF1 OPGs result from NF1 gene mutations, while sporadic OPGs arise from mutations such as BRAF fusion or BRAF-V600 mutations, resulting in varying tumour-related features and clinical behavior.

MRI allows for the visualization of underlying biological properties that result from cancer-related behavior. The apparent diffusion coefficient (ADC), indicating the magnitude of diffusion, can be useful in examining tissue characteristics in consequence of glioma activity (Nickerson et al., 2010). Glioma cell invasion/infiltration, not to be confused with proliferation (growth and division), is associated with increased values related to isotropic diffusion and ADC (Price et al., 2006) – this is postulated to be a result of infiltrative- and vascular-related edema and recruitment of microglia and reactive astrocyte activity. As such, in contrast to some other paediatric brain tumour subtypes, in which decreased ADC is often linked to more aggressive tumours (Hales et al., 2019; Tien et al., 1994), it has been suggested that OPGs with increased ADC values prior to treatment tend be more clinically aggressive, requiring earlier treatment (Yeom et al., 2013a). In addition, pilocytic astrocytomas exhibit prominent microvascular proliferation, and it has been shown that paediatric OPGs with increased histological microvascular density tend to undergo a higher rate of progression (Bartels et al., 2006). Perfusion-weighted MRI allows the hemodynamic properties of tumours to be measured *in vivo*, and some initial studies have suggested that increased vascular permeability (Jost et al., 2008), and potentially increased blood flow (Jittapiromsak et al., 2017), may be indicators of more aggressive OPG behavior.

The subventricular zone of the brain is a germinal niche, mainly composed of neural stem cells, precursor cells and migrating neuroblasts, where neurogenesis continues throughout adulthood (Alvarez-Buylla and García-Verdugo, 2002; Lim and Alvarez-Buylla, 2016) (Fig. 1). Due to the self-renewing ability of these cells, the subventricular zone of the lateral ventricle has been explored, *in-vivo* and with clinical MRI, as a role-player in gliomagenesis (Piccirillo et al., 2015), cancer cell infiltration (van Dijken et al., 2017) and patient outcome (Lim et al., 2007) in high-grade gliomas. Previous studies have identified a contributing role of the subventricular zone of the third ventricle (TVZ) in NF1-associated OPGs, and animal model experiments indicate that stem cells distally migrate to the optic nerve; after which they differentiate (Ono et al., 1997; Tchoghandjian et al., 2009). The location of the third ventricle, proximal to the hypothalamus and optic chiasm (Fig. 1B), notably raised interest in this zone in paediatric OPG (Dahiya et al., 2011) and it is now considered the location of NF1-associated OPG tumour cell origin (Dahiya et al., 2011; Lee et al., 2012; Tchoghandjian et al., 2009).

MRI can explore quantitative and qualitative imaging characteristics of the subventricular zone in relation to tumours, and MR-derived abnormalities in the subventricular zone proximal to the lateral ventricles have been demonstrated in both low-grade (Liu et al., 2016) and high-grade glioma (van Dijken et al., 2017). As the TVZ remains unexplored with MRI, and this is thought to be the germinal stem cell niche for OPGs, this study aimed to analyze MRI profiles surrounding the TVZ using diffusion- and perfusion-weighted MRI, in children with NF1-associated and sporadic OPG. Our aim was to determine whether quantitative MRI could identify imaging features of invasion in the TVZ of sporadic and NF1-associated OPG patients. As all previous studies utilize NF1-associated OPG models, particular interest was given to determining whether these MRI features existed in sporadic OPG. The objectives were 1) segment the transition zone by selecting voxels surrounding the TVZ; 2) compare ADC and cerebral blood flow (CBF) values surrounding the TVZ of NF1-associated and sporadic OPG patients, and examine how they compare to control participant TVZ data; and 3) explore possible associations of the TVZ imaging parameters with visual acuity measures, which served as a biomarker for how clinically aggressive the OPGs were in our cohort. The hypotheses were that TVZ imaging features in all OPG cases differ to that of controls; TVZ imaging features vary according to NF1 status; and imaging measures at the TVZ are associated with visual acuity measures in OPG patients. Specifically, given the known associations of elevated ADC and CBF with glioma invasion and infiltration, elevated ADC and CBF at the TVZ would correlate with a decline in visual function.

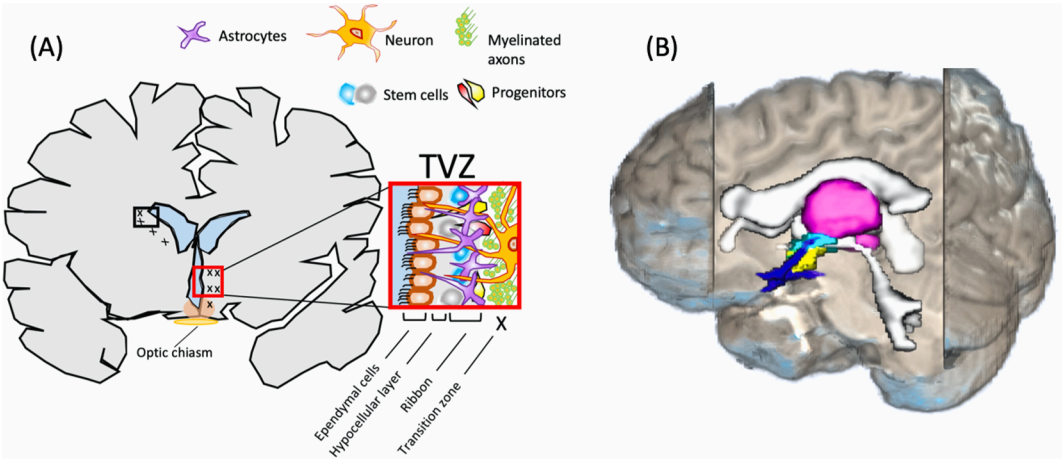

Fig. 1. (A) The subventricular zone of the third ventricle (TVZ) and its cytoarchitecture. The TVZ lines the ventricle and is composed of an ependymal later, an age-dependent hypocellular gap and an astrocytic ribbon which faces the transition zone into the parenchyma. The ependymal layer makes up the ventricle wall and is interiorly exposed to cerebral spinal fluid (blue) and exteriorly exposed to the hypocellular layer. In children, the sub-ependymal zone, which is composed of the hypocellular layer and astrocytic ribbon is a cellular collection ~3 mm in size. At the sub-ependymal zone, stem cells migrate outwards and/or downwards into the transition zone. In a normal setting, young optic pathway cells migrate via chain migration to the optic nerves, where their progenitors mature. In the cancer setting, cancer stem cells react to and interact with the parenchyma microenvironment and are classically known to invade rather than migrate. (B) Anatomical positioning of the TVZ relative to the third ventricle, thalamus, hypothalamus and optic pathway. The thalamus (magenta) surrounds the third ventricle and is located superior to the hypothalamus (yellow), which forms the inferior aspect and floor of the third ventricle, and also lies superior to the optic chiasm and optic tracts (blue). The TVZ (cyan) lines the inferior-lateral surface of the third ventricle and inferiorly runs through the lower aspect of the thalamus to the hypothalamus. In this figure, the TVZ is superimposed by the inferior component of hypothalamus. (For interpretation of the references to colour in this figure legend, the reader is referred to the web version of this article.)

2. Methods

2.1. Patients

Thirty patients with radiologically diagnosed OPG were included in this study, 20 of which were included in a previous study related to visual acuity and tractography of the optic pathway in OPG patients (Hales et al., 2017). Patients with NF1 were clinically and radiologically diagnosed according to current guidelines. All patients were receiving MRI assessment on a 3–6 monthly basis as well as regular ophthalmological monitoring. Institutional ethical approval was granted for this study. Data from 14 volunteer control participants were retrospectively acquired from an unrelated study, details of which are found in Stotesbury et al. (Stotesbury et al., 2018). Criteria for including control participants was that they be under the age of 18 years and healthy, with no evidence of neurological or psychiatric illness.

2.2. Ophthalmology evaluation

All patients were assessed by a paediatric ophthalmologist at our institution's ophthalmology clinic. Visual acuity (VA) was measured using age-appropriate testing methods, either Teller, logMAR Kays or logMAR. All VA scores were converted to the equivalent logarithm of the minimum angle of resolution (logMAR) score (Sloan, 1959), allowing for inter-patient comparison. On the logMAR chart, 20/20 vision is represented by the value 0, which increases with poorer vision, and the WHO defines a logMAR score of >0.5 as criteria for low vision. The logMAR score measured in each patient's best-performing eye (best-eye logMAR), worst-performing eye (worst-eye logMAR) and the mean of the best-eye and worst-eye values (mean logMAR) were recorded. Further analysis was based on mean logMAR values, as this was thought to best represent the overall quality of vision in a patient.

2.3. Magnetic resonance imaging

All imaging was performed on a Siemens 3.0 T Prisma scanner (Siemens, Erlangen, Germany), with a 20 channel head receive coil, as previously described (Hales et al., 2017). Our standard clinical MRI protocol included an axial T2-weighted turbo spin-echo acquisition, fluid attenuated inversion recovery sequences, and pre- and post-gadolinium T1-weighted acquisitions. Multi-shell diffusion and arterial spin labelling MRI was performed in conjunction with clinical protocols.

The multi-shell diffusion sequence included a diffusion-weighted spin-echo single shot 2D EPI acquisition [two shells: b = 1000, b = 2200; 2 × b_0 (one with phase-encoding flipped by 180° in the anterior-posterior direction); TR = 3050 ms; TE = 60 ms; FOV = 220 × 220 mm; matrix size = 110 × 110; in-plane voxel resolution = 2.0 mm; GRAPPA factor 2; phase-encoding partial Fourier = 6/8; scan time of 7 min 50 sec], as previously described (Hales et al., 2017).

Arterial spin labelling (ASL) data were acquired with a prototype pseudo-continuous-ASL (pCASL) sequence, the full details of which have been previously published (Hales et al., 2019). In brief, the sequence parameters were as follows: labelling duration = 1800 ms, post-labelling delay = 1500 ms, repetitions = 10, in-plane resolution 3.4 mm (interpolated to 1.7 mm), slice thickness = 4.0 mm, number of slices = 24. A proton-density weighted (M_0) image was also acquired (TR = 4000 ms), with identical readout to the ASL acquisition but with the labelling RF pulses removed, for CBF quantification. The total acquisition time was 3 min 19 sec.

2.4. Processing

Using *FSL* (FMRIB, Oxford), the susceptibility-induced off-resonance field was estimated and corrected by combining the diffusion-weighted data with the PE-flipped b_0 image, and eddy-current distortions were corrected. CBF maps were calculated in Matlab (Mathworks Inc., Natick, MA), following the guidelines described in the white paper by Alsop et al. (Alsop et al., 2015) (using $\lambda = 0.9$, $\alpha = 0.85$, $T_{1bl} = 1.65$ s).

Using the FSL FLIRT tool, all images were co-registered to the b_0 diffusion image using an affine registration with 12 degrees of freedom. The T2-weighted and T1-weighted post-contrast images were co-registered directly to the b_0. For the ASL data, the M_0 calibration image was co-registered to the b_0, and the transform matrix was applied to the CBF image.

2.5. Regions of interest

Tumour ROIs were manually segmented using MRview within the Mrtrix3 software package (Tournier et al., 2019), by a paediatric neuroradiologist with >4 years' experience (FD). Tumour segmentation was performed using the T2-weighted and T1-weighted post-contrast images for guidance (D'Arco et al., 2018). Paediatric OPGs do not consistently enhance on T1-weighted post-contrast images. The T1-weighted images were, therefore, used to guide the T2-weighted based tumour segmentation, as suggested previously (D'Arco et al., 2018). Subtle T2-weighted hyperintensities that completely lacked T1-weighted post-contrast enhancement and any mass effect were classified and segmented as focal abnormal signal intensities (FASI), previously termed unidentified bright objects, in NF1 cases.

The TVZ makes up a ~3 mm cellular lining along the latero-inferior base of the third ventricle (Dahiya et al., 2011). The parenchyma surrounding the TVZ makes up the transition zone along which new cells migrate. The TVZ transition zone was segmented in all patients and control participants. The third ventricle was identified using the b_0 images in all subjects. The TVZ-transition ROI was identified as the voxels surrounding the inferior-lateral walls and the floor of the third ventricle which were anatomically located at the transition between the thalamus and hypothalamus, running inferiorly to the base of the third ventricle. To minimize any partial volume effects of the CSF at the ventricle borders, a voxel-wide gap (2 mm) was applied along the ventricle lining, between the ventricle and the TVZ transition ROI (Fig. 2). TVZ ROI voxels that intersected with tumour or FASI voxels were excluded from analysis, with the aim of excluding CSF, tumour, and FASI voxels from the final TVZ transition ROI as far as possible. In a subset of 10 patients (5 NF1, 5 sporadic), a second reader independently defined the TVZ ROIs, and Dice scores (Dice, 1945) were used to assesses inter-reader agreement.

Mean ADC values, measured within the TVZ, were used in this study (TVZ ADC_{mean}). For CBF, previous studies have shown that the maximum value (rather than the mean) is best for examining tumour-related pathology (Aronen et al., 1994; Hales et al., 2019; Knopp et al., 1999; Law et al., 2003; Noguchi et al., 2008; Shin et al., 2002; Sugahara et al., 2001; Warmuth et al., 2003; Yeom et al., 2014), and as such the maximum CBF value in the TVZ was used in this study (TVZ CBF_{max}). Furthermore, TVZ ADC_{mean} and TVZ CBF_{max} values were normalized to the mean value from an ROI composed of normal-appearing grey matter in the frontal and temporal cortex in each patient (TVZ $nADC_{mean}$ and TVZ $nCBF_{max}$ respectively). This was done to cancel out 'global' changes in CBF and ADC between subjects, which might be due to age-related effects (Hales et al., 2014), as well as possible treatment-related effects. A further ROI, making up the entire normal-appearing grey matter cortex, was generated for each subject, so that these global changes in CBF and ADC could also be monitored.

2.6. Statistics

Data were analyzed with Matlab 2019b (Mathworks Inc, Natick, MA). Lilliefor's test was used to check for normality before comparing metrics between groups. Unpaired Student's t tests were used for normally-distributed data, and Mann-Whitney U-tests were used for non-normally distributed data. When analyzing differences between NF1-associated OPG patients, sporadic OPG patients, and control

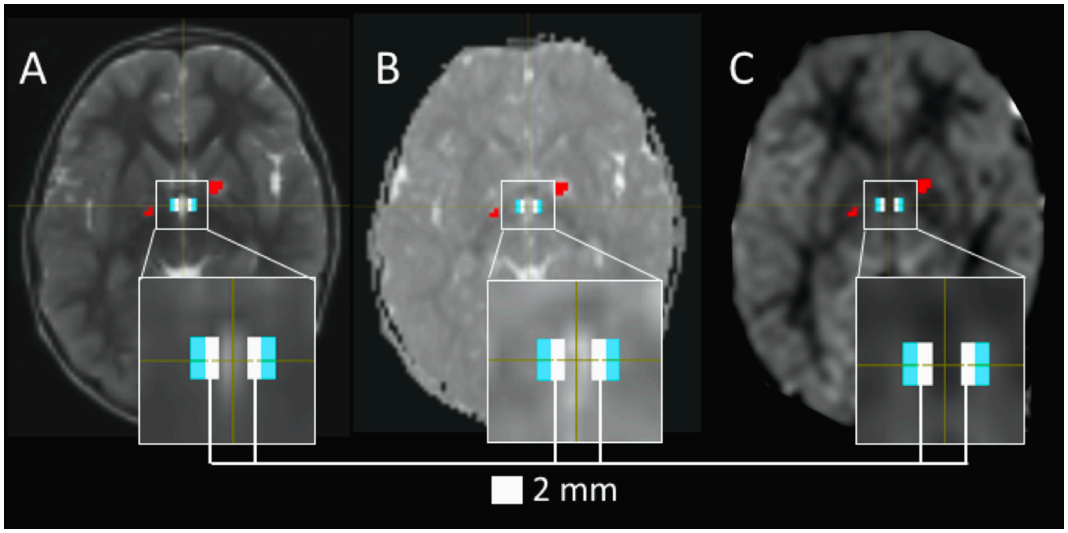

Fig. 2. Identifying voxels of the TVZ and eliminating partial volume effects in an NF1 patient. A 2 mm exclusion gap (white) was placed directly adjacent to the anterior-inferior aspect of the third ventricle wall, visualized on a T2-weighted image (A), and was confined by the anterior and posterior borders of the ventricle. The TVZ transition zone voxels (cyan) were placed directly adjacent to the exclusion gap. Measures of the ADC (B) and nCBF (C) in the TVZ voxels were collected. Focal abnormal signal intensities (red) and tumour were excluded from TVZ ROIs. (For interpretation of the references to colour in this figure legend, the reader is referred to the web version of this article.)

participants, one-way ANOVA tests were used, followed by a Tukey honestly significant difference post-hoc test to account for multiple comparisons. Significance was defined as $p < 0.05$ after multiple comparison correction. LogMAR scores were analyzed as continuous variables, and LogMAR scores for 'no perception of light' were assigned the value of 3.0 (Lee et al., 2010b).

Linear associations between TVZ $nADC_{mean}$ and TVZ $nCBF_{max}$ values and mean logMAR scores were explored independently in the NF1 and sporadic cohorts. In each group, the initial multivariate model included TVZ $nADC_{mean}$ and TVZ $nCBF_{max}$ as independent variables, and mean logMAR as the dependent variable. The independent variables were then eliminated in a step-wise manner, starting with the least significant variable, and continuing until only significant variables remained in the model.

3. Results

3.1. Clinical findings

Patient median age was 71 months (6 years; range 8 months – 17 years), and 15/30 (50%) patients were diagnosed with NF1. Visual acuity data were not available for 3 patients (1 NF1, 2 sporadic), and 2 further patients (both NF1) had an interval of more than 300 days between MRI and visual assessment (VA). These were excluded from the linear model examining associations between visual acuity and ADC/CBF. In the remaining patients (13 sporadic, 12 NF1), the median interval between MRI and VA was 16.5 days (range 1–189 days). Five patients (1 NF1, 4 sporadic) presented with no perception of light in their worst-performing eye, and measurable worst-eye vision ranged from 0.4 to 2.4 (median logMAR = 1.13). All patients had measurable vision in their best-performing eye (median logMAR = 0.26, range = −0.1–1.56). Control participant median age was 15 years (range 8–18 years), and VA data was not available for control subjects. After comparing the TVZ ROIs drawn by two independent readers, the median Dice score was 0.90, indicating a good level of agreement.

3.2. Comparisons between controls, sporadic and NF1 OPG patients

The full details of all group comparisons made between the controls, sporadic and NF1 OPG patients are given in Table 1. In summary, there were no significant group differences in the following parameters: cortical grey matter ADC ($p = 0.64$, one-way ANOVA); cortical grey matter CBF ($p = 0.53$, one-way ANOVA); number of patients on active treatment ($p = 0.47$, Fisher's exact test); number of patients with a tumour in the optic chiasm ($p = 0.11$, Fisher's exact test); interval between MRI and visual assessment ($p = 0.71$, Mann-Whitney *U* test); worst-eye logMAR ($p = 0.19$, Mann-Whitney *U* test); and mean logMAR ($p = 0.11$, Student's *t* test).

Subject age was significantly higher in the controls (mean 15.0 years), compared to the NF1 patients (mean 8.5 years, $p < 0.001$, one-

Table 1
Group comparisons between controls, sporadic and NF1 OPG patients. Statistical tests: a = Student's *t* test, b = Mann-Whitney *U* test, c = Fisher's exact test, d = one-way ANOVA.

	Sporadic	NF1	Control	p-value
No. subjects	15	15	14	N/A
Subject age (years)	5.29 ± 3.45	8.51 ± 4.61	15.03 ± 2.76	**<0.001**[d]
Active treatment	9/15	6/15	N/A	0.47[c]
GM ADC ($\times 10^{-3}$ mm^2/s)	0.80 ± 0.081	0.81 ± 0.056	0.82 ± 0.032	0.64[d]
TVZ $nADC_{mean}$	0.86 ± 0.10	0.95 ± 0.07	0.79 ± 0.06	**<0.001**[d]
GM CBF (ml/100 g/min)	53.85 ± 11.64	49.52 ± 11.24	49.84 ± 11.08	0.53[d]
TVZ $nCBF_{max}$	1.13 ± 0.25	0.92 ± 0.19	0.76 ± 0.11	**<0.001**[d]
TVZ volume (mm^3)	367.84 ± 212.07	492.80 ± 275.65	287.31 ± 42.86	**0.037**[d]
Tumour volume (mm^3)	1.85 ± 1.64 × 10^4	0.70 ± 1.58 × 10^4	N/A	**0.0028**[b]
Tumour in optic chiasm	13/15	8/15	N/A	0.11[c]
Patients with valid visual assessment	13/15	12/15	N/A	1.0[c]
MRI-VA interval (days)	26.33 ± 27.84	42.33 ± 57.09	N/A	0.71[b]
Best-eye logMAR	0.72 ± 0.53	0.25 ± 0.43	N/A	**0.021**[b]
Worst-eye logMAR	1.60 ± 1.07	1.18 ± 1.13	N/A	0.19[b]
Mean logMAR	1.16 ± 0.69	0.71 ± 0.65	N/A	0.11[a]

Statistical tests: a = Student's *t* test, b = Mann-Whitney *U* test, c = Fisher's exact test, d = one-way ANOVA.

way ANOVA) and sporadic patients (mean 5.3 years, $p < 0.001$, one-way ANOVA). TVZ volumes were significantly lower in the controls compared to the NF1 patients ($p = 0.03$, one-way ANOVA). Tumour volumes were larger in the sporadic group (18,452 ± 16,449 mm^3) compared to the NF1 group (6,967 ± 15,800 mm^3, $p = 0.003$, Mann-Whitney *U* test), and best-eye logMAR scores were also higher in the sporadic group (sporadic = 0.72 ± 0.53) compared to the NF1 group (0.25 ± 0.43, $p = 0.02$, Mann-Whitney *U* test).

3.3. TVZ group differences

Group differences in TVZ $nADC_{mean}$ and TVZ $nCBF_{max}$ values between the sporadic OPG patients, NF1 OPG patients, and controls, are shown in Fig. 3. The NF1-associated OPG group had significantly elevated TVZ $nADC_{mean}$ in comparison to sporadic ($p = 0.010$) and control participants ($p < 0.001$). TVZ $nCBF_{max}$ values in sporadic OPG patients were significantly elevated compared to that of NF1-associated OPG patients ($p = 0.016$), and control participants ($p < 0.001$).

3.4. Linear associations with vision

Significant findings from the linear regressions are illustrated in Fig. 4. In the NF1 OPG patients, after step-wise elimination of the non-significant independent variables, none of the variables remained as significant predictors of mean logMAR score. However, the negative correlation between TVZ $nCBF_{max}$ and mean logMAR fell just short of significance ($R^2 = 0.33$, $p = 0.051$, Fig. 4C). In the sporadic OPG patients, step-wise linear regression resulted in a final model in which a significant positive correlation was found between TVZ $nADC_{mean}$ and mean logMAR ($R^2 = 0.41$, $p = 0.019$, Fig. 4B), with this being the only significant predictor in the final model. A trend for a positive correlation between TVZ $nCBF_{max}$ and mean logMAR was observed, but this fell short of significance ($R^2 = 0.23$, $p = 0.095$, Fig. 4D).

4. Discussion

This study has demonstrated that a potential role may exist for quantitative MRI in the analysis of the TVZ transition zone in paediatric OPG. Utilizing known markers of tumour cell infiltrative activity, we explored the invasive profile at the TVZ, from where OPG cells originate and migrate. A correlation between this invasive profile and visual acuity was identified in sporadic OPG, suggesting that the microstructure of the TVZ in this group may be examined as a potential indicator of the tumour's behavioral phenotype in future studies. Our results suggest that the association between increased ADC and a more aggressive tumour phenotype may not be limited to the tumour itself, but may also apply to the TVZ in these patients. However, the fact that this correlation was not present in the NF1 patients is an area that warrants further study.

Sporadic OPG tend to be more clinically aggressive (Jost et al., 2008). In our study, tumour volumes were significantly higher in the sporadic group, and these patients had significantly poorer vision in their best-performing eye, compared to the NF1 OPG patients. As such, our results provide some additional evidence to suggest that sporadic OPGs represent a more clinically aggressive OPG phenotype.

Previous studies have reported elevated NF1 brain ADC in comparison to healthy controls (Eastwood et al., 2001). Post-mortem analyses of NF1 brains have reported increased fluid within the myelin, associated with hyper- or dysplastic glial cell proliferation (DiPaolo et al., 1995), as well as increased expression of glial fibrillary acid protein, indicative of reactive astrogliosis in the NF1 brain (Nordlund et al., 1995). This is supported by animal studies reporting global astrogliosis in NF1-knockout mice (Gutmann et al., 1999; Rizvi et al., 1999). In addition, a previous study identified reduced CBF in paediatric NF1 subjects compared to age-matched controls (Yeom et al., 2013b), most significantly in the posterior circulation and border zones of the middle and posterior cerebral arteries. It was postulated that this could be a result of either NF1-induced vasculopathy and associated steno-occlusive changes in the cerebral microvasculature, or alteration in cerebral metabolic demand.

In our study, no global differences in grey matter ADC or CBF were observed between the controls, sporadic OPG, and NF1 OPG patients. It should however be noted that only global grey matter values were recorded in this study, and more localized differences may have been present. We did however observe higher normalized ADC values in the TVZ in the NF1 OPG patients, compared to the sporadic OPG patients and controls. In the sporadic OPG patients, normalized CBF values in the TVZ were higher than both the NF1 OPG patients and controls. As these values were normalized to normal-appearing grey matter in the same brain, these findings were specific to the TVZ, rather than reflecting any global changes.

The increased CBF in the TVZ of sporadic patients may be linked to the higher microvascular density which has been observed in more aggressive OPGs, which are typically sporadic (Bartels et al., 2006). However, the same cannot be said of ADC, as if higher ADC values are indeed linked with OPGs which tend be more clinically aggressive, as suggested in (Yeom et al., 2013a), we might have expected increased ADC values in the TVZ in sporadic patients as well. It could be that this

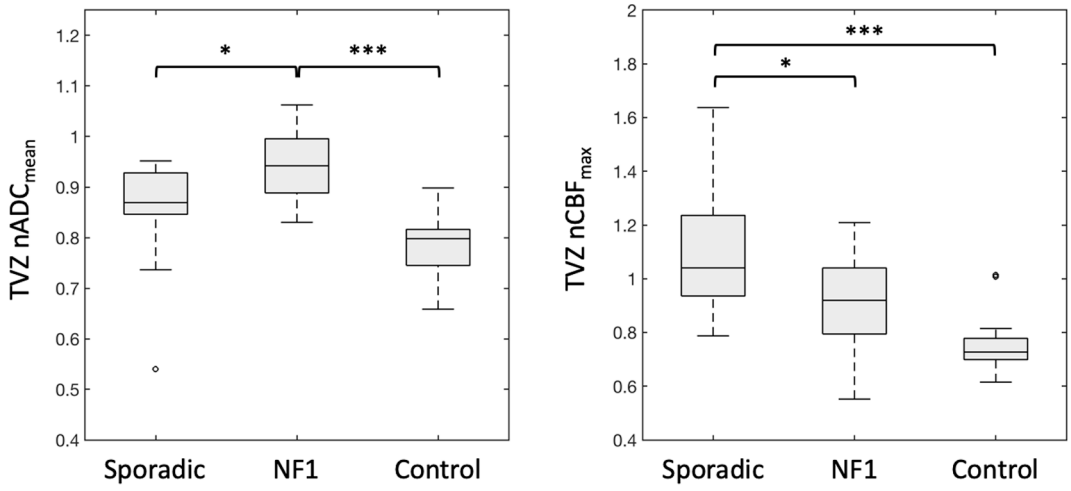

Fig. 3. Boxplots comparing TVZ $nADC_{mean}$ and TVZ $nCBF_{max}$ values in sporadic OPG patients, NF1-associated OPG patients, and control participants. Significant differences are indicted in the figure: * $p < 0.05$, *** $p < 0.001$.

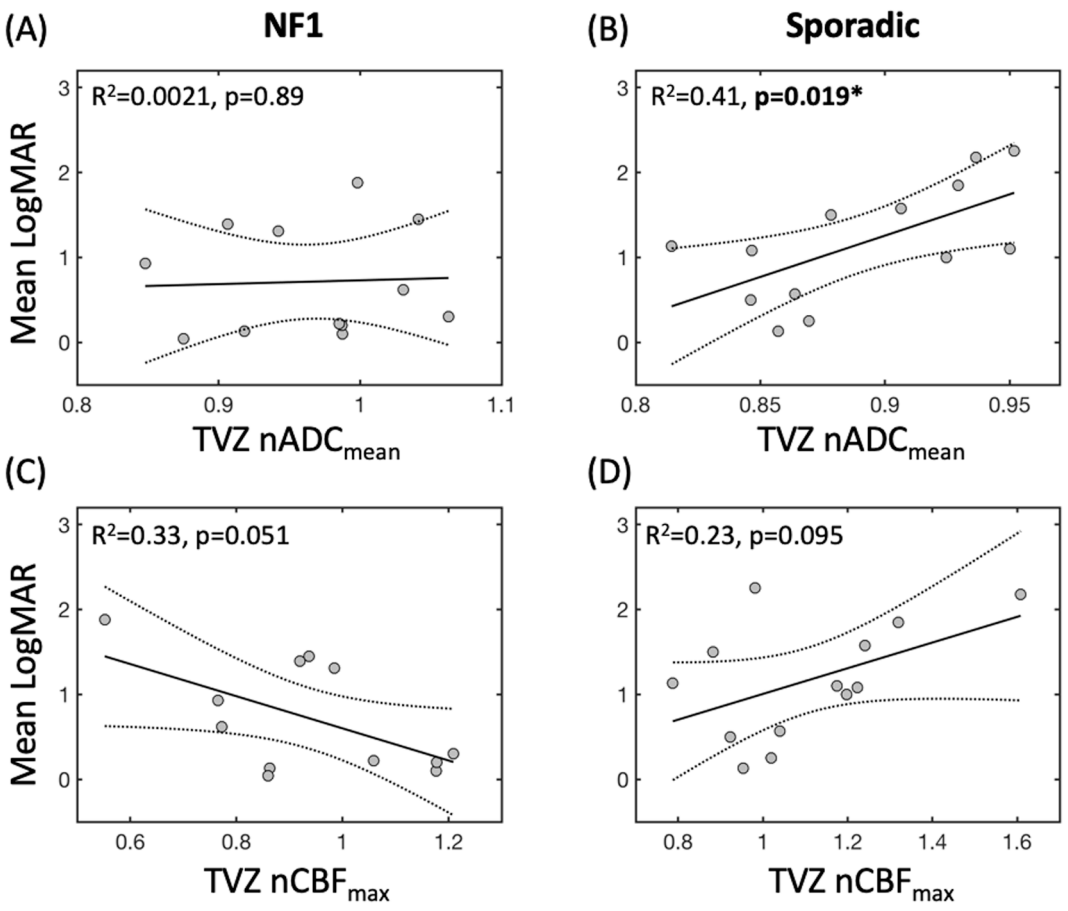

Fig. 4. Scatter plots summarizing TVZ $nCBF_{max}$ and $nADC_{mean}$ correlations with mean logMAR score, in NF1-associated and sporadic OPG patients. The best-fit and confidence interval lines from the linear models are illustrated, along with the R^2 and p values for model.

instead reflects a more localized manifestation of the aforementioned reactive astrogliosis processes observed in the NF1 brain. However, further work is needed to fully understand the underlying mechanisms resulting in the differences observed in the TVZ between sporadic and NF1 OPG patients in this study.

Our study had a number of limitations. Our single-center cohort was relatively small and included data from 30 patients. However, OPGs are rare and comprise only 3% of all paediatric cranial tumours, and our center is the largest referral center in the UK. Age differences existed between the controls and OPG patients. However, by using TVZ ADC and CBF values which were normalized to normal-appearing grey matter in the same brain, age-related changed should be cancelled out in this study. In addition, it would have been ideal to include an additional control group in this study, comprising NF1 subjects without an OPG, in order to separate innate differences in the NF1 brain from those associated with OPGs. However, this was not possible as MRI scans in asymptomatic patients with NF1 were not available. As such, we were unable to conclude whether the differences seen in the TVZ between NF1 and sporadic OPG patients are only applicable in the presence of a tumour, or whether the same differences would be appreciable in NF1 subjects without an OPG. Furthermore, the hypotheses presented here focus on the microenvironment that potentially exists at the TVZ transition zone and, as this was an MRI study, we cannot directly address concepts relating to cell-of-origin. However, it is our understanding that *in vivo* cell-of-origin studies are underway in other institutions. Lastly, the segmentation of OPG in NF1 comes with a unique set of limitations that involve the existence of FASI. To address this, FASI- and tumour-associated voxels were excluded to the best of our ability, with the intention of focusing the analysis exclusively on the TVZ.

In conclusion, quantitative MRI can identify features at the TVZ transition zone that differ between OPG patients with NF1, patients with a sporadic OPG, and healthy controls. To our knowledge, we are the first to utilize MRI to probe features within this region in the context of paediatric OPG, and to provide preliminary evidence of a correlation between the cellular properties of the TVZ (as assessed by MRI), and tumour aggressiveness (as assessed by visual loss) in the sporadic OPG setting. Our findings indicate that patients with NF1-associated and sporadic OPG, despite having tumours which are thought to be histologically indistinguishable, display distinguishable MRI profiles at the TVZ. Further work is needed to investigate the biology of the TVZ microenvironment in the context of NF1 and sporadic OPG patients, and to determine if these differences persist in NF1 subjects in which no OPG is present.

Funding

This work was funded by Great Ormond Street Hospital Children's Charity (W1075B) and Children with Cancer UK (grant number CwCUK-15-203).

CRediT authorship contribution statement

Natalie R. Boonzaier: Conceptualization, Methodology, Software, Formal analysis, Investigation, Writing - original draft, Writing - review & editing, Visualization. **Patrick W. Hales:** Methodology, Software, Formal analysis, Investigation, Writing - original draft, Writing - review & editing, Visualization, Supervision, Funding acquisition. **Felice D'Arco:** Formal analysis, Writing - review & editing, Resources.

Bronwen C. Walters: Resources. **Ramneek Kaur:** Data curation, Project administration. **Kshitij Mankad:** Writing - review & editing, Resources. **Jessica Cooper:** Resources. **Alki Liasis:** Resources. **Victoria Smith:** Resources. **Patricia O'Hare:** Resources. **Darren Hargrave:** Writing - review & editing, Funding acquisition. **Christopher A. Clark:** Writing - review & editing, Supervision, Funding acquisition, Project administration.

Declaration of Competing Interest

The authors declare that they have no known competing financial interests or personal relationships that could have appeared to influence the work reported in this paper.

Acknowledgements

This work was supported by the National Institute for Health Research Biomedical Research Centre at Great Ormond Street Hospital for Children NHS Foundation Trust and University College London.

References

Alsop, D.C., Detre, J.A., Golay, X., Günther, M., Hendrikse, J., Hernandez-Garcia, L., Lu, H., MacIntosh, B.J., Parkes, L.M., Smits, M., van Osch, M.J.P., Wang, D.J.J., Wong, E.C., Zaharchuk, G., 2015. Recommended implementation of arterial spin-labeled perfusion MRI for clinical applications: a consensus of the ISMRM perfusion study group and the European consortium for ASL in dementia. Magn. Reson. Med. 73, 102–116. https://doi.org/10.1002/mrm.25197.

Alvarez-Buylla, A., García-Verdugo, J.M., 2002. Neurogenesis in adult subventricular zone. The Journal of neuroscience 22, 629–634. https://doi.org/0270-6474/02/220629-06.

Aronen, H.J., Gazit, I.E., Louis, D.N., Buchbinder, B.R., Pardo, F.S., Weisskoff, R.M., Harsh, G.R., Cosgrove, G.R., Halpern, E.F., Hochberg, F.H., 1994. Cerebral blood volume maps of gliomas: comparison with tumor grade and histologic findings. Radiology 191, 41–51. https://doi.org/10.1148/radiology.191.1.8134596.

Bartels, U., Hawkins, C., Ma, J., Ho, M., Dirks, P., Rutka, J., Stephens, D., Bouffet, E., 2006. Vascularity and angiogenesis as predictors of growth in optic pathway/hypothalamic gliomas. J. Neurosurg.: Pediatrics 104, 314–320. https://doi.org/10.3171/ped.2006.104.5.314.

Dahiya, S., Lee, D.Y., Gutmann, D.H., 2011. Comparative characterization of the human and mouse third ventricle germinal zones. J. Neuropathol. Exp. Neurol. 70, 622–633. https://doi.org/10.1097/NEN.0b013e31822200aa.

D'Arco, F., Culleton, S., De Cocker, L.J.L., Mankad, K., Davila, J., Tamrazi, B., 2018. Current concepts in radiologic assessment of pediatric brain tumors during treatment, part 1. Pediatr. Radiol. 48, 1833–1843. https://doi.org/10.1007/s00247-018-4194-9.

Dice, L.R., 1945. Measures of the amount of ecologic association between species. Ecology 26, 297–302. https://doi.org/10.2307/1932409.

DiPaolo, D.P., Zimmerman, R.A., Rorke, L.B., Zackai, E.H., Bilaniuk, L.T., Yachnis, A.T., 1995. Neurofibromatosis type 1: pathologic substrate of high-signal-intensity foci in the brain. Radiology 195, 721–724. https://doi.org/10.1148/radiology.195.3.7754001.

Eastwood, J.D., Fiorella, D.J., MacFall, J.F., Delong, D.M., Provenzale, J.M., Greenwood, R.S., 2001. Increased brain apparent diffusion coefficient in children with neurofibromatosis type 1. Radiology 219, 354–358. https://doi.org/10.1148/radiology.219.2.r01ap25354.

Gutmann, D.H., Loehr, A., Zhang, Y., Kim, J., Henkemeyer, M., Cashen, A., 1999. Haploinsufficiency for the neurofibromatosis 1 (NF1) tumor suppressor results in increased astrocyte proliferation. Oncogene 18, 4450–4459. https://doi.org/10.1038/sj.onc.1202829.

Hales, P.W., D'Arco, F., Cooper, J., Pfeuffer, J., Hargrave, D., Mankad, K., Clark, C., 2019. Arterial spin labelling and diffusion-weighted imaging in paediatric brain tumours. NeuroImage. Clinical 22, 101696. https://doi.org/10.1016/j.nicl.2019.101696.

Hales, P.W., Kawadler, J.M., Aylett, S.E., Kirkham, F.J., Clark, C.A., 2014. Arterial spin labeling characterization of cerebral perfusion during normal maturation from late childhood into adulthood: normal 'reference range' values and their use in clinical studies. J. Cereb. Blood Flow Metab. 34, 776–784. https://doi.org/10.1038/jcbfm.2014.17.

Hales, P.W., Smith, V., Dhanoa-Hayre, D., O'Hare, P., Mankad, K., D'Arco, F., Cooper, J., Kaur, R., Phipps, K., Bowman, R., Hargrave, D., Clark, C., 2017. Delineation of the visual pathway in paediatric optic pathway glioma patients using probabilistic tractography, and correlations with visual acuity. NeuroImage: Clinical. https://doi.org/10.1016/j.nicl.2017.10.010.

Jittapiromsak, N., Hou, P., Liu, H.-L., Sun, J., Slopis, J.M., Chi, T.L., 2017. Prognostic role of conventional and dynamic contrast-enhanced MRI in optic pathway gliomas. J. Neuroimaging 27, 594–601. https://doi.org/10.1111/jon.12450.

Jost, S.C., Ackerman, J.W., Garbow, J.R., Manwaring, L.P., Gutmann, D.H., McKinstry, R.C., 2008. Diffusion-weighted and dynamic contrast-enhanced imaging as markers of clinical behavior in children with optic pathway glioma. Pediatr. Radiol. 38, 1293–1299. https://doi.org/10.1007/s00247-008-1003-x.

Knopp, E.A., Cha, S., Johnson, G., Mazumdar, A., Golfinos, J.G., Zagzag, D., Miller, D.C., Kelly, P.J., Kricheff, I.I., 1999. Glial neoplasms: dynamic contrast-enhanced T2*-weighted MR imaging. Radiology 211, 791–798.

Kornreich, L., Blaser, S., Schwarz, M., Shuper, A., Vishne, T.H., Cohen, I.J., Faingold, R., Michovitz, S., Koplewitz, B., Horev, G., 2001. Optic pathway glioma: correlation of imaging findings with the presence of neurofibromatosis. Am. J. Neuroradiol. 22, 1963–1969.

Law, M., Yang, S., Wang, H., Babb, J.S., Johnson, G., Cha, S., Knopp, E.A., Zagzag, D., 2003. Glioma grading: sensitivity, specificity, and predictive values of perfusion MR imaging and proton MR spectroscopic imaging compared with conventional MR imaging. AJNR Am. J. Neuroradiol. 24, 1989–1998.

Lee, D.Y., Gianino, S.M., Gutmann, D.H., 2012. Innate neural stem cell heterogeneity determines the patterning of glioma formation in children. Cancer Cell 22, 131–138. https://doi.org/10.1016/j.ccr.2012.05.036.

Lee, D.Y., Yeh, T.-H., Emnett, R.J., White, C.R., Gutmann, D.H., 2010a. Neurofibromatosis-1 regulates neuroglial progenitor proliferation and glial differentiation in a brain region-specific manner. Genes Dev. 24, 2317–2329. https://doi.org/10.1101/gad.1957110.

Lee, J.W.Y., Lai, J.S.M., Yick, D.W.F., Tse, R.K.K., 2010b. Retrospective case series on the long-term visual and intraocular pressure outcomes of phacomorphic glaucoma. Eye 24, 1675–1680. https://doi.org/10.1038/eye.2010.108.

Lim, D.A., Alvarez-Buylla, A., 2016. The adult ventricular-subventricular zone (V-SVZ) and olfactory bulb (OB) neurogenesis. Cold Spring Harbor Perspect. Biol. 8, a018820 https://doi.org/10.1101/cshperspect.a018820.

Lim, D.A., Cha, S., Mayo, M.C., Chen, M.-H., Keles, E., VandenBerg, S., Berger, M.S., 2007. Relationship of glioblastoma multiforme to neural stem cell regions predicts invasive and multifocal tumor phenotype. Neuro-Oncology 9, 424–429. https://doi.org/10.1215/15228517-2007-023.

Listernick, R., Ferner, R.E., Liu, G.T., Gutmann, D.H., 2007. Optic pathway gliomas in neurofibromatosis-1: Controversies and recommendations. Ann. Neurol. 61, 189–198. https://doi.org/10.1002/ana.21107.

Liu, S., Wang, Y., Fan, X., Ma, J., Ma, W., Wang, R., Jiang, T., 2016. Anatomical involvement of the subventricular zone predicts poor survival outcome in low-grade astrocytomas. PLoS ONE 11, e0154539. https://doi.org/10.1371/journal.pone.0154539.

Nickerson, J.P., Salmela, M.B., Koski, C.J., Andrews, T., Filippi, C.G., 2010. Diffusion tensor imaging of the pediatric optic nerve: Intrinsic and extrinsic pathology compared to normal controls. J. Magn. Reson. Imaging 32, 76–81. https://doi.org/10.1002/jmri.22228.

Noguchi, T., Yoshiura, T., Hiwatashi, A., Togao, O., Yamashita, K., Nagao, E., Shono, T., Mizoguchi, M., Nagata, S., Sasaki, T., Suzuki, S.O., Iwaki, T., Kobayashi, K., Mihara, F., Honda, H., 2008. Perfusion imaging of brain tumors using arterial spin-labeling: correlation with histopathologic vascular density. Am. J. Neuroradiol. 29, 688–693. https://doi.org/10.3174/ajnr.A0903.

Nordlund, M.L., Rizvi, T.A., Brannan, C.I., Ratner, N., 1995. Neurofibromin expression and astrogliosis in neurofibromatosis (type 1) brains. J. Neuropathol. Exp. Neurol. 54, 588–600.

Ono, K., Yasui, Y., Rutishauser, U., Miller, R.H., 1997. Focal ventricular origin and migration of oligodendrocyte precursors into the chick optic nerve. Neuron 19, 283–292. https://doi.org/10.1016/S0896-6273(00)80939-3.

Piccirillo, S.G.M., Sottoriva, A., Watts, C., 2015. The role of sub-ventricular zone in gliomagenesis. Aging 7, 738–739. https://doi.org/10.18632/aging.100823.

Price, S.J., Jena, R., Burnet, N.G., Hutchinson, P.J., Dean, A.F., Peña, A., Pickard, J.D., Carpenter, T.A., Gillard, J.H., 2006. Improved delineation of glioma margins and regions of infiltration with the use of diffusion tensor imaging: An image-guided biopsy study. Am. J. Neuroradiol. 27, 1969–1974. https://doi.org/10.1016/S0513-5117(08)79144-0.

Rizvi, T.A., Akunuru, S., de Courten-Myers, G., Switzer, R.C., Nordlund, M.L., Ratner, N., 1999. Region-specific astrogliosis in brains of mice heterozygous for mutations in the neurofibromatosis type 1 (Nf1) tumor suppressor. Brain Res. 816, 111–123. https://doi.org/10.1158/0008-5472.CAN-09-2490.

Shin, J.H., Lee, H.K., Kwun, B.D., Kim, J.-S., Kang, W., Choi, C.G., Suh, D.C., 2002. Using relative cerebral blood flow and volume to evaluate the histopathologic grade of cerebral gliomas: preliminary results. AJR Am. J. Roentgenol. 179, 783–789. https://doi.org/10.2214/ajr.179.3.1790783.

Sloan, L.L., 1959. New test charts for the measurement of visual acuity at far and near distances. Am. J. Ophthalmol. 48, 807–813.

Stotesbury, H., Kirkham, F.J., Kölbel, M., Balfour, P., Clayden, J.D., Sahota, S., Sakaria, S., Saunders, D.E., Howard, J., Kesse-Adu, R., Inusa, B., Pelidis, M., Chakravorty, S., Rees, D.C., Awogbade, M., Wilkey, O., Layton, M., Clark, C.A., Kawadler, J.M., 2018. White matter integrity and processing speed in sickle cell anemia. Neurology 90, e2042–e2050. https://doi.org/10.1212/WNL.0000000000005644.

Sugahara, T., Korogi, Y., Kochi, M., Ushio, Y., Takahashi, M., 2001. Perfusion-sensitive MR imaging of gliomas: comparison between gradient-echo and spin-echo echo-planar imaging techniques. AJNR Am. J. Neuroradiol. 22, 1306–1315.

Tchoghandjian, A., Fernandez, C., Colin, C., El Ayachi, I., Voutsinos-Porche, B., Fina, F., Scavarda, D., Piercecchi-Marti, M.-D., Intagliata, D., Ouafik, L., Fraslon-Vanhulle, C., Figarella-Branger, D., 2009. Pilocytic astrocytoma of the optic pathway: a tumour deriving from radial glia cells with a specific gene signature. Brain 132, 1523–1535. https://doi.org/10.1093/brain/awp048.

Tien, R.D., Felsberg, G.J., Friedman, H., Brown, M., MacFall, J., 1994. MR imaging of high-grade cerebral gliomas: value of diffusion-weighted echoplanar pulse

sequences. AJR Am. J. Roentgenol. 162, 671–677. https://doi.org/10.2214/ajr.162.3.8109520.

Tournier, J.-D., Smith, R., Raffelt, D., Tabbara, R., Dhollander, T., Pietsch, M., Christiaens, D., Jeurissen, B., Yeh, C.-H., Connelly, A., 2019. MRtrix3: A fast, flexible and open software framework for medical image processing and visualisation. NeuroImage 202, 116137. https://doi.org/10.1016/j.neuroimage.2019.116137.

van Dijken, B.R.J., Yan, J.-L., Boonzaier, N.R., Li, C., van Laar, P.J., van der Hoorn, A., Price, S.J., 2017. Subventricular zone involvement characterized by diffusion tensor imaging in glioblastoma. World Neurosurgery 105, 697–701. https://doi.org/10.1016/j.wneu.2017.06.075.

Warmuth, C., Günther, M., Zimmer, C., 2003. Quantification of blood flow in brain tumors: comparison of arterial spin labeling and dynamic susceptibility-weighted contrast-enhanced MR imaging. Radiology 228, 523–532. https://doi.org/10.1148/radiol.2282020409.

Yeom, K.W., Lober, R.M., Andre, J.B., Fisher, P.G., Barnes, P.D., Edwards, M.S.B., Partap, S., 2013a. Prognostic role for diffusion-weighted imaging of pediatric optic pathway glioma. J. Neurooncol. 113, 479–483. https://doi.org/10.1007/s11060-013-1140-4.

Yeom, K.W., Lober, R.M., Barnes, P.D., Campen, C.J., 2013b. Reduced cerebral arterial spin-labeled perfusion in children with neurofibromatosis type 1. AJNR Am. J. Neuroradiol. 34, 1823–1828. https://doi.org/10.3174/ajnr.A3649.

Yeom, K.W., Mitchell, L.A., Lober, R.M., Barnes, P.D., Vogel, H., Fisher, P.G., Edwards, M.S., 2014. Arterial spin-labeled perfusion of pediatric brain tumors. AJNR Am. J. Neuroradiol. 35, 395–401. https://doi.org/10.3174/ajnr.A3670.